



### **Concours du réseau vision**

**Candidat :** Matthieu Vanni, étudiant au PhD (sup. C. Casanova), axe Cerveau/Perception  
Laboratoire des Neurosciences de la Vision  
École D'Optométrie. Université de Montréal

**Titre de l'article :** Evaluation of receptive field size from higher harmonics in visuotopic mapping using continuous stimulation optical imaging. *Journal of Neuroscience Methods* 189 (2010) 138–150

### **Biographie :**

Après un cursus à l'École Normale Supérieure (Paris), Matthieu Vanni s'est spécialisé dans le domaine des neurosciences à l'Université Pierre & Marie Curie (DEA, Paris 6). Très intéressé par les aspects qu'apportent les nouvelles technologies d'imagerie cérébrale, il a par la suite suivi une formation complémentaire en imagerie biomédicale à l'Institut de Formation d'Ingénieurs en Techniques Électroniques (DESS Imagerie Électronique). Cette formation double lui a permis d'occuper un poste d'assistant de recherche au Commissariat à l'Énergie Atomique en France où il a pu participer au développement d'un dispositif d'imagerie nucléaire pour la recherche animale actuellement commercialisé par la société Biospace Lab.

Depuis 2004, il a débuté un PhD en Sciences Biomédicales à l'Université de Montréal pour travailler sur la quantification et l'étude du rôle des cartes corticales dans le système visuel (financé par le ministère des affaires étrangères du Canada et l'Université de Montréal). L'étude *in vivo* de l'organisation détaillée du cortex nécessite l'emploi de méthodes d'imagerie extrêmement résolutive sur de larges portions de cerveau que seule l'imagerie optique des signaux intrinsèques peut offrir. C'est pour cette raison qu'il a rejoint le laboratoire de Christian Casanova à l'École d'Optométrie qui possède une des plateformes de ce type les plus avancées du Canada (financements IRSC, CRSNG et NIH). Depuis 2006, il a également engagé une collaboration très étroite avec le laboratoire de Frédéric Lesage à l'École Polytechnique pour développer des projets en rapport avec l'élaboration de méthodes quantitatives en imagerie optique. Une de ces études a d'ailleurs été primée par le FRSQ l'année dernière. L'article présenté ici, traite d'un autre des aspects développés lors de cette collaboration :

Depuis les années 90, l'imagerie optique des signaux intrinsèques est la technique d'imagerie fonctionnelle qui a permis d'obtenir la meilleure résolution spatiale sur de large portion de cortex. Toutefois, son signal est majoritairement contaminé par la forte contribution des bruits vasculaires. De nombreuses stratégies ont donc été élaborées pour réduire cette participation, dont récemment une approche basée sur la présentation périodique des stimuli couplée à un enregistrement continu des images et une analyse spectrale de la réponse dans le temps (*stimulation continue*). Cette approche a permis d'augmenter de 10x le niveau de rapport signal / bruit mais n'a jusqu'ici jamais pris en compte la contribution du couplage neurovasculaire et ne s'est limité jusqu'ici qu'à une analyse à une seule harmonique ce qui a considérablement limité son emploi et la pertinence des mesures. Dans l'article présenté ici, un modèle a été élaboré afin d'évaluer le profil de la réponse neuronale en prenant en compte le couplage neurovasculaire et la réponse mesurée à de multiples harmonique. Cette approche a permis d'évaluer la taille

des champs récepteurs en se basant sur la largeur de la réponse optique au passage d'une barre. Ce nouveau paradigme d'évaluation de la carte des tailles de champs récepteurs pourra donc représenter un outil fondamental dans les études s'intéressant à l'impact de certaines pathologies dans l'intégration spatiale des neurones de la rétine et du cerveau telles que le glaucome.

After an initial education at the “Ecole Normale Supérieure (Paris)”, Matthieu Vanni specialized in the field of neurosciences at the University Pierre & Marie Curie (DEA, Paris 6). Interested in the opportunities that new methods in brain imaging provide, he decided to complete his formation by an additional training in biomedical imaging (DESS in electronic imaging). This double skill allowed him to occupy a position of research assistant at the « Commissariat à l’Énergie Atomique » in France where he had participated to the development of a nuclear imaging device for animal research currently distributed by Biospace Lab.

Since 2004, he has begun a PhD in Biomedical Sciences at the University of Montreal to work on the quantification and the description of cortical maps in the visual system (supported by the Government of Canada and the University of Montreal). The study of the precise organization of the cortex in vivo requires the use of high resolution imaging methods from large portions of brain that only optical imaging of intrinsic signals can provide. For this reason, he joined the Casanova Lab at the School of Optometry which has the most advanced imaging platform of this type in Canada (funding CIHR, NSERC and NIH). Since 2006, he has also worked very closely with the laboratory of Frederic Lesage at the Polytechnic to develop projects related to the development of quantitative methods in optical imaging. The article presented here deals with one aspect developed during this collaboration:

Since the 90s, optical imaging of intrinsic signals is the functional imaging technique that has yielded the best spatial resolution over large portions of cortex. However, signal is mainly contaminated by the strong contribution of vascular noises. Many strategies have been developed to reduce this contribution, including a recent approach based on the periodic stimuli coupled to a continuous recording of images and spectral analysis of the response over the time. This approach has led to an increase of 10x the signal to noise ratio but has so far not taken into account the contribution of neurovascular coupling and is only limited to the analysis of a single harmonic. In the article presented here, a model was developed to assess the neural response profile, taking into account the neurovascular coupling and the response to multiple harmonics. This approach was used to assess the size of receptive fields based on the width of the optical response for a drifting bar. This new evaluation paradigm of the receptive field size map may therefore be a fundamental tool for studies looking at the impact of some diseases in the spatial integration of neurons in the retina or brain such as glaucoma.



## Evaluation of receptive field size from higher harmonics in visuotopic mapping using continuous stimulation optical imaging

Matthieu P. Vanni<sup>a,b</sup>, Jean Provost<sup>c</sup>, Frédéric Lesage<sup>c</sup>, Christian Casanova<sup>a,\*</sup>

<sup>a</sup> Laboratoire des Neurosciences de la Vision, École d'optométrie, Université de Montréal, CP 6128, succ. Centre-ville, Montréal, Québec, Canada H3C 3J7

<sup>b</sup> Faculté de Médecine, Université de Montréal, Montréal, Québec, Canada

<sup>c</sup> École Polytechnique de Montréal, Département de génie électrique et Institut de génie biomédical, Montréal, Québec, Canada

### ARTICLE INFO

#### Article history:

Received 8 December 2008

Received in revised form 17 March 2010

Accepted 17 March 2010

#### Keywords:

Area 17  
Area 18  
Bandwidth  
Cat  
Continuous stimulation  
Cortical map  
Fourier  
Hemodynamic response  
Intrinsic signals  
Optical imaging  
Orientation  
Receptive field  
Visuotopy  
Visual cortex

### ABSTRACT

The extraction and detection of specific responses from a large amount of background noise has been the subject of a considerable body of research in brain functional imaging, and more specifically in optical intrinsic signal imaging. Recent work by Kalatsky and Stryker (2003) showed that by combining different conditions and using periodic stimuli, recording times can be reduced. Spectral decomposition is then used to provide amplitude and phase information locked to the stimulus. A drawback of the above method is that by focusing only on a single harmonic, response information is limited. The shape of the hemodynamic response function (HRF) and the temporal variations in the neural responses cannot be assessed. In this work it is argued that additional information about neural responses can be gathered by using higher harmonics. Moving bars were used to generate visuotopic maps on large portions of the cat visual cortex. Up to four simultaneously bars moving repetitively across the visual field at different frequencies were used to sample the HRF in the Fourier domain. The HRF profile obtained with continuous stimulation was spatially homogeneous throughout the cortex and similar to the HRF profile obtained using episodic stimulation. Furthermore, by modeling the optical response as a convolution between HRF and neuronal responses, the ratio of the second harmonic to the first provided an estimation of the receptive field size. This was further validated by measuring spatial frequency selectivity. Therefore, the use of higher harmonics opens new avenues to estimate receptive field size from temporal signals.

© 2010 Elsevier B.V. All rights reserved.

### 1. Introduction

The extraction and detection of specific visual responses from a large amount of background noise remains a challenge in intrinsic optical imaging. In the literature, averaging or differential imaging methods (used in episodic paradigm) are generally used (Blasdel, 1992) and are probably the simplest means to extract neuronal maps. Averaging a number of repetitions exploits the fact that sources of physiological periodic noise (i.e., heartbeat, respiration and vasomotion) are not synchronized with the stimulation (Mayhew et al., 1996). Refinements on these analyses such as signal decomposition by principal components analysis have been subsequently developed (Everson et al., 1997; Gabbay et al., 2000). More recently, time-locked or periodic techniques which infer responses from amplitude and phase information locked to the stimulus have been explored (Sornborger et al., 2003, 2005). For example,

using these principles, Kalatsky and Stryker (2003) revealed precise visuotopic maps of the visual cortex. In contrast to the episodic technique, the continuous stimulation paradigm allows the combination of different conditions by periodically changing the stimuli recovering the spatial response by using phase information at the stimulation frequency. Experiment duration is thus considerably reduced since, as in case of visuotopic studies, an “infinite” number of stimulus positions can be presented with a high signal to noise ratio (SNR). However, the detection method considers the response elicited at only a single frequency, and consequently, for most stimuli, remains limited in terms of information content. As an example in the context of visuotopic maps described above, current periodic models fail to provide any knowledge about the size of the underlying receptive fields' population (pRF).

In this study, techniques developed for the analyses of fMRI-images and event related diffuse optical signal (Cohen-Adad et al., 2007; Marrelec et al., 2003) are used to model periodic optical signals by introducing a canonical hemodynamic response function (HRF). We will show that, by including higher harmonics in periodic techniques, this hemodynamic model provides a mean to extract additional information from the acquired data, such as HRF

\* Corresponding author. Tel.: +1 514 343 2407; fax: +1 514 343 2382.

E-mail address: [christian.casanova@umontreal.ca](mailto:christian.casanova@umontreal.ca) (C. Casanova).

URL: <http://www.opto.umontreal.ca/neurosciences/> (C. Casanova).

profile and pRF size. Results are validated in four steps: first, the hemodynamic model is validated with the “continuous stimulation paradigm” used to create visuotopic maps at a sub-millimeter scale of the cat primary visual cortex. Second, the linearity of the optical responses is investigated by combining multiple stimuli in one recording session. Third, multiple stimuli data is used to evaluate the profile of the hemodynamic response and compared to that obtained from episodic stimulation. Finally, harmonics are used to evaluate pRF size (i.e., second/first harmonic ratio). Part of this work has been previously published in abstract form (Vanni et al., 2007).

## 2. Methods

### 2.1. Signal model

The model presented in this work is based on the periodic stacking method (Sornborger et al., 2005) and is further developed by including a model of the HRF. Although the HRF can vary between animals and spatially in the cortex, it is useful to assume at first that it is known. A discussion of how to either estimate it or the limitations of the procedure will follow. The model will then be used to estimate responses and to show how higher harmonics can be used to infer new information from the underlying signal.

For intrinsic optical imaging, a camera is positioned over the cortex to image a zone where activation patterns are expected (Bonhoeffer and Grinvald, 1996). The cortex is illuminated uniformly by light, at one or more wavelengths for which hemoglobin dominates the absorption (Dunn et al., 2005). The images are recorded continuously to form a dynamical image  $I(t)$  for each illumination wavelength  $\lambda$ . Only one  $\lambda$  is modeled in this work assuming that a combination of deoxyhemoglobin (HbR) and oxy-hemoglobin (HbO) is measured. For a pixel in the image,  $\{ij\}$ , the measured attenuation can be modeled as the sum of the stimulus response and physiological (e.g., vasomotion, respiration, heart-beat) and acquisition (e.g., generated by the camera) noises,

$$I_{ij}(t) = \alpha_{ij} HRF_{ij}(t) \times R_{ij} \{s(x, y, t)\} (t) + b_{ij}(t) + e_{ij}(t), \quad (1)$$

where  $e_{ij}$  represents the acquisition noise that can be white or structured,  $b_{ij}$  describes the physiological noise at each point. The specificity of the neuronal response is defined by a period-normalized function described by the functional  $R_{ij}\{s(x,y,t)\}(t)$  (the bracket denotes the functional dependence). The functional  $R_{ij}\{s(x,y,t)\}(t)$  describes the shape of the neuron response to a given stimulus  $s(x,y,t)$ . In the specific case of a moving bar used in this paper, the functional can be expressed as a convolution. However the notation extends to cases where the dependence is not convolutional, as would be the case with stimuli consisting of contrast changes. In the latter case, the specificity takes the form of a sigmoid function with respect to contrast.  $s(x,y,t)$  represents the stimulation vector defined on the stimulus plane  $\{x,y\}$ , such as a computer monitor showed to the subject.  $\alpha_{ij}$  is a real number representing the amplitude of the response.  $R_{ij}\{s(x,y,t)\}(t)$  is a function of time and of the cortex spatial coordinates  $\{ij\}$ . Its exact form will depend on the stimulus  $s(x,y,t)$ ,  $HRF_{ij}(t)$  is the hemodynamic response function that convolves the stimuli.

Typically, stimulus-locked paradigms are designed such that their spatial extent can be entirely parameterized by a temporal variable and a stimulation frequency  $\omega_1$ . The model (1) is sufficiently general to be applied to a wide range of stimuli such as RDK, etc. (Vanni et al., 2010). However, for illustrative purposes, we will consider, throughout this paper, vertical bar stimuli. In this case, the repetition  $n$  of a vertical bar stimulus of width  $X$  centered at the position  $\{x_0, y_0\}$  at  $t=0$  and displayed on a screen of height  $H$

and width  $L$  can be written as a function of time alone:

$$\begin{aligned} s(x, y, t) &= \text{rect} \left( \frac{\frac{L}{2\pi}(\omega_1 t + 2\pi n) - x_0}{X} \right) \text{rect} \left( \frac{y_0}{H} \right) \\ &= \text{rect} \left( \frac{\frac{L}{2\pi}\omega_1(t - t_0 + \frac{2\pi n}{\omega_1})}{X} \right) \times 1 = s(t; \omega_1) \end{aligned} \quad (2)$$

where  $t_0$  is given by  $x_0/L\omega_1$  and can be assumed to be zero without loss of generality,  $\text{rect}((x-a)/2b)$  is a function equal to 1 in  $[a-b, a+b]$  and 0 elsewhere.

When measuring the phase and amplitude of the temporal Fourier transform (denoted by the symbol  $\hat{\cdot}$ ) of  $I_{ij}(t)$  we then obtain

$$\hat{I}_{ij}(\omega) = \alpha_{ij} H \hat{R}F_{ij}(\omega) \hat{R}_{ij} \{s(t; \omega_1)\} (\omega) + \hat{b}_{ij}(\omega) + \hat{e}_{ij}(\omega) \quad (3)$$

Since the physiological noise is important only in a subset of frequencies, e.g. vasomotion (Mayhew et al., 1996), the first term of the above expression will dominate the measured signal at  $\omega_1$  if it is chosen outside this subset. Typically, the amplitude and phase of the temporal Fourier transform of the dynamic image at the stimulation frequency  $\omega_1$ ,  $\hat{I}_{ij}(\omega_1)$ , are used to generate isochrones of the cortical response. Within our model this Fourier transform is given by

$$\hat{I}_{ij}(\omega_1) = \alpha_{ij} |H \hat{R}F_{ij}(\omega_1) \hat{R}_{ij} \{s(t; \omega_1)\} (\omega_1)| e^{i\omega_1(\varphi - \tau_{ij})} \quad (4)$$

keeping in mind that this equation is valid only at frequencies away from physiological noise and where we assumed that  $e_{ij}$  was negligible. The phase of the response is composed of two components. A first component, interpreted as a delay  $\tau_{ij}$  that may be different from point to point depending on stimuli. A second term, denoted by  $\phi$  in the expression above, accounts for hemodynamic phases or other parameters (such as  $t_0$ ) that are intrinsic to the local response. Therefore, in periodic paradigms, the phase can be exploited to identify a given activation with a stimulus state, for example spatial position.

To optimize continuous stimulation paradigms, we first note that although non-sinusoidal stimuli operate at a single frequency, their Fourier transform will contain information at other frequencies. Moreover, the Fourier transform of the HRF is non zero on a finite domain and is smooth (Ciuciu et al., 2003). Although it is expected that this function may vary among animals, cortical areas and under the influence of anesthesia, those variations have been shown to be smaller across areas than across subjects (Handwerker et al., 2004).

### 2.2. Response model

The objective of this section is to be more specific about the information that can be extracted from such formalism by utilizing the phase and amplitude of the measured signal at different harmonics, i.e.,  $\omega_1, 2\omega_1, 3\omega_1, 4\omega_1$ , etc. First, a typical continuous stimulation is modeled by a periodic stimulus, such as a vertical bar moving horizontally. Previous work modeled the associated response as a sinusoidal function, and estimation methods have been used to recover its amplitude (Sornborger et al., 2003, 2005). This formalism was shown to be successful in increasing the SNR and decreasing the acquisition time required to get neuronal maps. However more information can be extracted from the measured signal when the model used takes into account the HRF and the neuronal specificity to the stimulus. In the following, both these components will be introduced in two steps: first, an idealistic response of a neuron (or a group of neurons), perfectly specific to the preferred stimulus (e.g., the position of the vertical bar), is revisited by modeling its temporal impulse response with a Dirac

distribution. Second, the approach is then generalized to a more realistic Gaussian-like response around that preferred stimulus.

An idealistic period-normalized neural response to a preferred stimulus consisting of a periodically moving bar with period  $T = \omega_1/2\pi$  can be modeled by a response of infinite amplitude of the group of neuron corresponding to pixel  $\{ij\}$  when the center of the bar reaches a location  $\tau_{ij}$ , i.e.  $t - \frac{2\pi n}{\omega_1} = \tau_{ij}$ , and is zero otherwise. This can be written using a truncated Dirac comb, i.e., a sum of equally spaced Dirac delta functions,

$$R_{ij} \{s(t; \omega_1)\} (t) = \sum_{n=0}^N \delta(t - \frac{2\pi n}{\omega_1} - \tau_{ij}) \quad (5)$$

where  $n$  is the stimulus repetition index and  $N$  is the total number of stimulus periods presented (the total acquisition time can thus be expressed as  $NT$ ),  $t$  is time and  $\tau_{ij}$  is the time at which the neurons respond to this stimulus within the period, i.e., at which bar position they are perfectly specific. The periodic stimulation leads to harmonic components in the Fourier transform of (5) with the amplitude of the harmonic located at the stimulation frequency,  $\omega_1$ , being linearly dependant on this number of periods  $N$  (see Appendix A for details):

$$|\hat{I}_{ij}(\omega_1)| = \alpha_{ij} |H\hat{R}F_{ij}(\omega_1)| (N + 1). \quad (6)$$

This equation simply states the fact that the longer the periodic stimulus, the higher the amplitude at the stimulus frequency will be. When this expression is combined with a simple assumption on the spectral structure of physiological noise, it can be used to optimize stimulation frequencies. While (6) focused on the stimulation frequency,  $\omega_1 = 2\pi/T$ , the same expression can be evaluated at multiples of the stimulus frequency,  $\omega_q = q\omega_1$  giving

$$|\hat{I}_{ij}(\omega_q)| = \alpha_{ij} |H\hat{R}F_{ij}(\omega_q)| (N + 1) \quad (7)$$

In this expression, the ideal response (5) contributes equally in amplitude to all harmonics. However, the Fourier transform of the HRF, which decays with higher frequencies, will lead to decreasing amplitudes with increasing frequency. The only additional information contained in those harmonics is related to the HRF itself.

While the model above is instructive, modeling  $R\{s(t; \omega_1)\}(t)$  by a truncated Dirac comb as above is not accurate. In the visual cortex, neurons will be selectively activated in a certain range  $\sigma_{ij}$  around their preferred position. This is in accordance with the concept of neuron selectivity being associated with a portion of the visual field, the receptive field (Hubel and Wiesel, 1962). Moreover, given that one pixel in the optical image represents the activity of not one but several neurons, that their receptive field position is scattered and that intrinsic optical signals comprise spiking and sub-threshold activity as well as pre- and post-synaptic signals, the response of one pixel will be considered as the response of a population of receptive fields (named pRF thereafter), (Albus, 1975; Buzas et al., 2003; Cynader et al., 1987; Das and Gilbert, 1997, 1995; Zepeda et al., 2004). The use of pRF is even more appropriate as there are “point spread” functions due to the spatial extent of the capillary blood supply (Dunn et al., 2005) and light scattering in cortex (Polimeni et al., 2005).

It thus becomes reasonable to consider a Gaussian-shaped neuronal stimulus response with standard deviation  $\sigma_{ij}$  around a given position to model those effects. A convolution in the time domain corresponds to a multiplication in the Fourier domain and the Fourier transform of the Gaussian function is also a Gaussian function with an inversely proportional width. Thus, adding a Gaussian-shaped response modeling neuronal specificity convolved with the stimulus-driven ideal response acts as a low-pass filter altering higher frequency harmonics in the frequency domain. Explicitly, for a given pixel with a response width  $\sigma_{ij}$ , the modeled

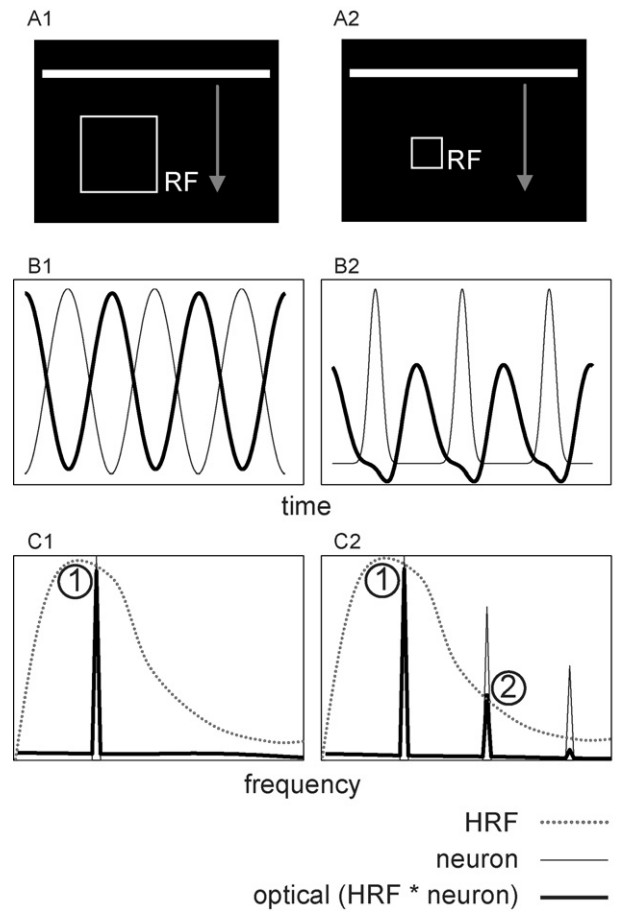


**Fig. 1.** (A) Schematic representation of the stimuli (bars moving downward) in the visual field and receptive fields (white squares; RF). (B) Simulation of representative optical (thick lines) and neuronal (thin lines) responses in two situations: large (B1) and small (B2) receptive fields. The optical response corresponds to the response of the neuronal population convolved by the HRF. (C) Fourier transform of the responses presented in B. The HRF envelope is represented by dotted lines. The numbers (1 and 2) represents first and second harmonics.

$\hat{R}_{ij}^G \{s(t; \omega_1)\} (\omega)$  becomes:

$$\hat{R}_{ij}^G \{s(t; \omega_1)\} (\omega) = e^{-\frac{1}{2}\omega^2\sigma_{ij}^2} \hat{R}_{ij} \{s(t; \omega_1)\} (\omega) \quad (8)$$

This additional parameter increases the model complexity but can also be used to access new information. Fig. 1 summarizes heuristic expectations from this model by casting the width  $\sigma_{ij}$  in terms of the receptive field size (squares). Two situations are presented, in the first situation, (panel A1), the receptive field is large while in the second, (panel A2), it is small. By convolving the neural responses with the HRF, the temporal responses (row 2) and their effect in the spectral domain (row 3) for the two situations (row 1) are presented. For small receptive fields (panel A2), there is a change in the response temporal profile (panel B2) associated with an increase of the amplitude of the second harmonic which is apparent from the asymmetry created by the convolved response. The change in harmonic amplitudes is thus a signature of variations in pRF size. This signature can be exploited to quantify receptive field size.

This heuristic description above can be recast in a quantitative estimate. For example, it is possible to evaluate  $\sigma_{ij}$  by using the amplitude of the Fourier coefficients of the harmonics. First, as shown in (8) and (4), modeling receptive field size amounts to multiplying (6) by a Gaussian function in the frequency domain. Expressing the temporal Fourier transform  $|\hat{I}_{ij}(\omega)|$  at  $\omega_1$

and  $\omega_2 = 2\omega_1$  (assuming noises are negligible at both harmonics), taking the ratio ( $|I_{ij}(\omega_2 = 2\omega_1)|/|I_{ij}(\omega_1)|$ ) and rearranging the terms, we can isolate the width parameter as

$$\begin{aligned}\sigma_{ij}^2 &= \frac{2}{\omega_1^2 - \omega_2^2} \ln \left( \frac{|HRF(\omega_1)I_{ij}(\omega_2)|}{|HRF(\omega_2)I_{ij}(\omega_1)|} \right) \\ &= \frac{-2}{3\omega_1^2} \ln \left( \frac{|HRF(\omega_1)I_{ij}(2\omega_1)|}{|HRF(2\omega_1)I_{ij}(\omega_1)|} \right)\end{aligned}\quad (9)$$

Note that in the last equation, even if there is no knowledge of the real HRF, the ratio of frequencies  $|HRF(\omega_1)|/|HRF(2\omega_1)|$  can be hypothesized to be constant over the observed region of interest (ROI). Under this hypothesis, the change from one cortical location to another depends solely on the changes of the measured signal, allowing mapping this parameter or comparing surface of pRF ( $\sigma^2$ ) between two regions A and B.

$$\sigma_A^2 - \sigma_B^2 = \frac{-2}{3\omega_1^2} \ln \left( \frac{|I_A(2\omega_1)I_B(\omega_1)|}{|I_A(\omega_1)I_B(2\omega_1)|} \right)\quad (10)$$

In expressions above, the response temporal width,  $\sigma_{ij}$ , is used. However, it is not a natural parameter in the brain but it is directly related to the receptive field angular width  $\sigma_{ij}'$  expressed as:

$$\sigma_{ij}' = \frac{\sigma_{ij}\omega_1}{2\pi\Delta\theta}\quad (11)$$

With  $\Delta\theta$  describing the overall experiment angular range in the visual field leading to

$$\sigma_A^2 - \sigma_B^2 = \frac{-1}{3\pi\omega_1\Delta\theta} \ln \left( \frac{|I_A(2\omega_1)I_B(\omega_1)|}{|I_A(\omega_1)I_B(2\omega_1)|} \right)\quad (12)$$

This last expression will be validated by comparing the results obtained with standard techniques below. The direct quantitative application of (9) is not straightforward since it requires an estimate of the HRF at both harmonic frequencies. Expression (12) however can be used without difficulty providing quantitative 2D maps of relative pRF. In the next section, the single frequency stimulation paradigm is extended to evaluate the HRF in the Fourier domain with this model.

### 2.3. Hemodynamic response estimation

The formalism developed in the previous section allows the use of higher harmonics to gain insight into neuronal specificity. In this section, the feasibility of estimating the HRF with a set of harmonics is studied. Previous results have shown that it is possible to superimpose two stimuli at different frequencies and recover independently both related activity maps (Kalatsky et al., 2006). Assuming linearity and using the model above, the response for multiple stimuli is written as the sum of responses for single stimulus

$$R_{ij}^G \left\{ \sum_{k=1}^{nstim} s_k(t; \omega_k) \right\} (t) = \sum_{k=1}^{nstim} R_{ij}^G \{ s_k(t; \omega_k) \} (t)\quad (13)$$

Where  $nstim$  describes the number of stimuli used. Let  $T_k$  be the periods of the different stimuli,  $N_k$  be the number of periods for each type of stimulus that occur in a fixed experiment total time,  $T_{exp}$ , i.e.  $N_k = T_{exp}/T_k$ . By using  $N_k \gg 1$  and ensuring that response components are distinguishable in order to respect the linearity condition (in other words, the  $\omega_k$ 's must not be multiples of one another), the HRF of a pixel in the image can be sampled in the frequency domain. This is shown by observing that at a given pixel, the amplitude of the Fourier transform of (13) at the frequency of

the  $p$ -th stimulus is dominated by that stimulus (see Appendix A for details)

$$\left| \hat{R}_{ij}^G \left\{ \sum_{k=1}^{nstim} s_k(t; \omega_k) \right\} (\omega_p) \right| \approx e^{\frac{1}{2}\omega_p^2\sigma_p^2} (N_p + 1)\quad (14)$$

where the influence of the tails of the Gaussian functions coming from the other stimuli on the harmonics of stimulus  $p$  have been neglected. The spatial angular response described in Eq. (11) is the same for all stimuli, i.e.  $\omega_k\sigma_k = \omega_l\sigma_l$  for all  $k, l$  at a given pixel  $\{ij\}$ . Thus at the first harmonic of each stimulus frequency,  $\omega_p = 2\pi/T_p$ , the exponential term in (14) will have the same value, that is

$$\beta = e^{\frac{1}{2}\omega_p^2\sigma_p^2} = e^{\frac{1}{2}\omega_k^2\sigma_k^2}\quad (15)$$

The effect of the width is thus the same for each stimulus frequency and the measured signal will be affected by the same constant  $\beta$ , i.e.

$$|\hat{I}_{ij}(\omega_p)| \approx \alpha_{ij}\beta |HRF(\omega_p)| (N_p + 1)\quad (16)$$

Up to this constant, dividing the signal at each frequency by  $(N_p + 1)$  results in measures of the amplitude of the Fourier transform of the HRF at each  $\omega_p$ . Effective sampling can be done, for instance, with multiple horizontal bars moving vertically at different speeds. However, the choice of stimulus frequencies must be done judiciously. Choosing an equispaced sampling of the frequency domain is not a good idea as explained above since the responses would be summed at multiples of the stimulation frequency. Moreover, the harmonics will be affected by the  $\sigma_{ij}$ 's and cannot be used to get more sampling points in this estimation without estimating  $\omega_k\sigma_k$  first. An estimation of the modulus of the HRF with (16) is still possible by using a minimization process based on a parametric form of the HRF. The parametric form minimized consists of two gamma functions used to describe the delays of the response and ensuing undershoot, their dispersion as well as the ratio of the response to the undershoot. It is based on the canonical HRF originating from fMRI (from SPM2, <http://www.fil.ion.ucl.ac.uk/spm/software/spm2/>). While the family of curves described by the SPM parametric form may not always be adapted to optical imaging, since a combination of HbO and HbR is measured, it should be noted however that at 630 nm, the wavelength used in the experiments, the extinction coefficient of HbR is 10 times larger than that of HbO<sub>2</sub> supporting this choice since Blood Oxygen Level Dependent (BOLD) fMRI is more sensitive to HbR.

This procedure is described in Appendix B and results are presented below.

### 2.4. Animal preparation

Six adult cats were used in this study (2.5–3.5 kg). All procedures were made in accordance with the guidelines of the Canadian Council for the Protection of Animals, and the experimental protocol was accepted by the Ethics committee of the University of Montreal. Throughout the experiment, the animal was placed in a stereotaxic frame and artificially ventilated with a mixture of halothane (Fluothane<sup>®</sup>, 0.6–0.8%) in O<sub>2</sub>/N<sub>2</sub>O (30%/70%). Muscular relaxation was obtained by the continuous injection of gallaminetriethiodide (2%) infused with 5% dextrose in lactated Ringer's injection solution. End-tidal CO<sub>2</sub> level, blood pressure, blood oxygen saturation, core temperature (feed-back controlled), electroencephalogram and electrocardiogram were continuously monitored to evaluate the depth of anesthesia and adjust ventilation. Pupils were dilated with atropine sulfate 1% (Isopto<sup>®</sup>) and the eyes were protected using contact lenses of appropriate refractive power. An antibiotic (Tribissen 24%, 0.125 mL/kg/day) was injected s.c. to prevent

infections. A 27 mm × 20 mm craniotomy was performed over the primary visual cortex (areas 17, 18 and 19) at Horsley Clarke coordinates AP –10 to +17 and ML –10 to +10, and the dura was incised to access the cortex. A stainless steel imaging chamber was positioned over the craniotomy, filled with silicone oil and sealed with a glass cover slip. At the end of each experiment, the animal was killed by an intravenous overdose of pentobarbital sodium (Euthanyl, ~100 mg/kg).

### 2.5. Acquisition and stimulation

The cortex was illuminated at 545 nm to locate the surface vascular pattern and at 630 nm to record the intrinsic signals. Images were acquired with a 12 bits CCD camera (1M60, Dalsa, Colorado Springs, USA) fitted with a macroscopic lens (Nikon, AF Micro Nikkor, 60 mm, 1:2.8D). For continuous stimulation sessions, acquisition lasted 10–30 min (2–8 Hz sampling frequency). Full-screen visual stimuli were generated using a custom made software and presented on a computer subtending 120 × 90 degrees of visual angle. The blind spot was back projected on the computer screen with a light source and used to determine the position of the *area centralis* (Bishop et al., 1962).

As in the paradigm described in Kalatsky and Stryker (2003), periodic activations were obtained with light bars (width of 5°, luminance of 50 cd/m<sup>2</sup>) moving horizontally or vertically on a dark background at frequencies varying from 0.03 to 0.5 Hz. Visuotopy and  $\sigma^2$  were evaluated with one or three bars moving at a fixed frequency. The evaluation of the HRF was derived from the combination of four bars moving simultaneously but at different frequencies. In the latter case, five sets of stimulation were recorded with distinct frequencies; first set: 0.06, 0.11, 0.15 and 0.20 Hz, second set: 0.03, 0.08, 0.13 and 0.17 Hz, third set: 0.04, 0.09, 0.15 and 0.19 Hz, fourth set: 0.07, 0.12, 0.18 and 0.21 Hz and fifth set: 0.23, 0.32, 0.42 and 0.50 Hz. To compare the data from one set to another and form an HRF independently of external conditions (e.g. anesthesia), common frequencies were chosen between pairs of experiments and used to normalize the data between sets. The rationale behind using five sets of four bars is as follows. To measure the HRF, a sufficient sampling of the frequency axis is necessary to provide substantial information about the response. However, the number of bars could not be increased much more because the stimuli may be interpreted differently by the cortex (i.e. since several bars will be simultaneously within an individual receptive field) and the linear hypothesis used would not stand.

Classical episodic protocols were used to validate different parts of the study. Spatial frequency selectivity maps were obtained from orientation maps evoked with eight spatial frequency gratings: 0.05, 0.1, 0.15, 0.25, 0.35, 0.75 and 1.0 c/deg. For each spatial frequency, vertical and horizontal orientations were presented during 8 s (1.6 s per frame) and spaced by 10 s during which the next stationary stimulus was presented. Each of these 16 conditions was randomly presented 30 times. The episodic HRF was evoked by a 0.15 c/deg grating pseudo-randomly presented 50 times during 3 s at two orthogonal orientations, preceded and followed by an equiluminant blank screen. The frame acquisition began 5 s before and lasted 12 s after the stimulation onset (total = 80 frames, each lasting 20 s).

### 2.6. Offline pre-processing and episodic analysis

Data were imported into Matlab (The Mathworks, Natick, MA) for further analysis. Signals were subtracted by a normalized temporal pattern of lighting instability to account for illumination variations. A Fourier transform was performed on the temporal signal for each pixel to obtain phase and magnitude spectra. For continuous HRF estimation, baselines of spectra, corresponding to

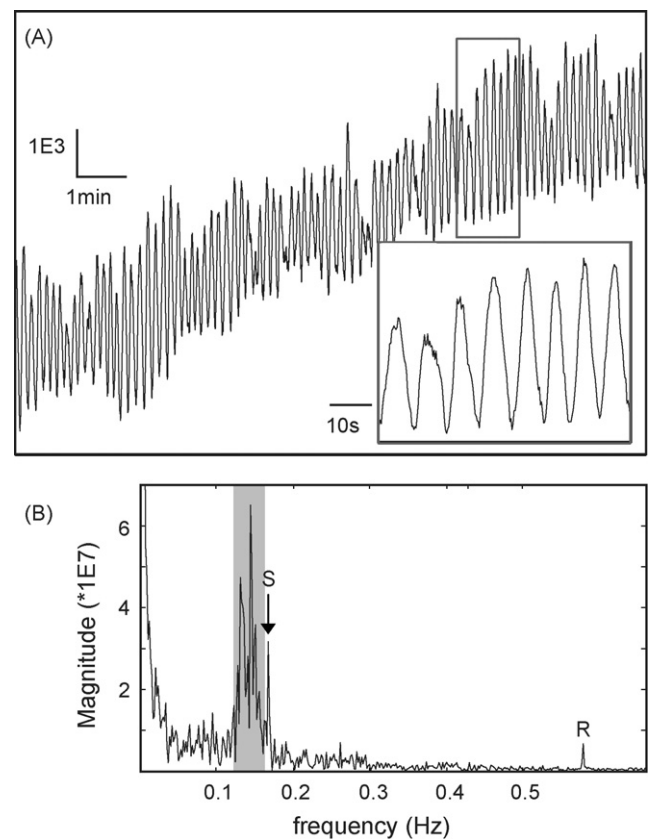


**Fig. 2.** (A) Raw signal recorded in one location of the cortex from case 1 (corresponding to the red circle in Fig. 3, panel A) during a 10-min period. Note the large amplitude of the vasomotion waves. (B) Fourier transform magnitude spectrum of the signal where three components are clearly visible: stimulus (S, 0.167 Hz), vasomotion waves (approximately defined by a grey box around 0.14 Hz) and respiration (R, 0.6 Hz). In the present case, there were no signals at the second harmonic because of the stimulus frequency and pRF size, as explained in the Section 2.

the noise floor, were subtracted to reduce the contribution of physiological components. The comparison with the episodic HRF was done as follows: a least-squared fit to a Gaussian mixture model containing three or four components (to describe the phases of the HRF (Chen-Bee et al., 2007)) was performed on the modulus of each harmonic component. This fit was then compared to the measured episodic waveform to assess its validity. To estimate the spatial uniformity of the HRF in the cortex, a correlation analysis was done for each point between the estimated HRF (averaged over all points) and the harmonics measured at each location.

For the spatial frequency evaluation, trial responses were averaged and band-pass filtered to remove low and high frequency noise. Absolute value of the difference between activation for horizontal and vertical gratings was measured for each spatial frequency. Optimal spatial frequency was evaluated with a modified Gaussian function for each pixel as previously described in (Villeneuve et al., 2009). For the episodic HRF estimation, responses for all orientations and trials were summed and no additional processing was performed.

## 3. Results

### 3.1. Visuotopic mapping of the visual cortex

As a first step to the analysis proposed in the previous section, we confirmed that visuotopic maps could be obtained in cats with the continuous paradigm. Fig. 2 displays the raw data used to compute these maps. The temporal profile of the raw signal recorded in

one location of area 18 shows a major contribution of vasomotion (large periodic fluctuations observed in panel A). A slow drift is also observed that is probably due to instrumentation (light source and camera heating). By performing the Fourier transforms on this signal, different components could be discriminated: the response to the stimulus (a bright horizontal bar moving periodically through the visual field at 0.17 Hz), vasomotion waves distributed around 0.14 Hz as they are not purely periodic and respiration at 0.6 Hz (panel B). The vasomotion waves varied in amplitude, but their frequencies were always greater than 0.1 Hz. The Fourier transform also provides a phase value related to the response delays that can be used to determine the visuotopy time-delayed by the HRF. The resulting phase map (for elevation) is shown in panel B of Fig. 3. Since phase alone is not always associated to a significant response, an improved representation of the visuotopy in the primary visual cortex was obtained by normalizing the phase by the signal amplitude. This is presented in panel C and in the [supplementary video 1](#). The main part of the primary visual cortex accessible for imaging was area 18, and in particular the regions representing the central and lower parts of the visual field. A limited portion of area 17, representing the central part of the visual field, was visible in the posterior part. According to the phase transition, a drift of visuotopy along the elevation was seen in the anterior–posterior axis with the lower part of the visual field represented in the anterior part of the visual cortex (panel C). Using a vertical bar, the same cortical surface was activated along the azimuth, revealing the contralateral representation of the visual field in both hemispheres (panel D and [supplementary video 2](#)). Similar results were obtained in all animals tested (see [supplementary Fig. 1](#)). In near half of the cases tested, a decrease of the cortical magnification factor was observed along the mediolateral axis i.e., cortical zones progressively representing the peripheral parts of the visual field along the azimuth. These visuotopic discontinuities (e.g. “patches” or “islands”) are indicated by white arrows in panel D of Fig. 2. A similar organization was also described by (Albus and Beckmann, 1980). [Supplementary Fig. 2](#) shows the visuotopy (panels A and B) corrected by the hemodynamic delay (see Methods in Kalatsky and Stryker (2003)) and illustrates the visuotopic organization with elevation and azimuth isobars superimposed on the anatomical picture (panel C). When three bars moving at the same frequency were presented, the response amplitude was increased. In this configuration, the recording time needed to accurately map visuotopy was reduced to less than one minute (compares panels B and D and see SNR measures in panel E of [supplementary Fig. 1](#)). It is worth pointing out that the use of multiple bars drifted at the same frequency induces an unsolvable uncertainty about the phase locked to the visual representation and should be avoided for exact visuotopic mapping.

### 3.2. HRF estimation

A refinement of the technique was made by using different frequencies of stimulation in a given recording session (Fig. 4). The aim was to confirm the possibility to measure several responses simultaneously and thus, to reduce the time necessary to estimate the HRF. When two bars were drifted perpendicularly, visuotopy along azimuth and elevation could be mapped from two periodic components (panels A and [supplementary video 3](#)). Two responses were also evoked and easily discriminated when two horizontal bars moved in opposite directions (panels B and [supplementary video 4](#)). Finally, two bars moving in the same direction at different frequencies yielded comparable elevation visuotopic maps, but shifted by two distinct frequency-dependent HRF delays (panels C and [supplementary video 5](#)).

Up to four bars moving at different frequencies were successfully used to estimate HRF in the same recording session. Fig. 5

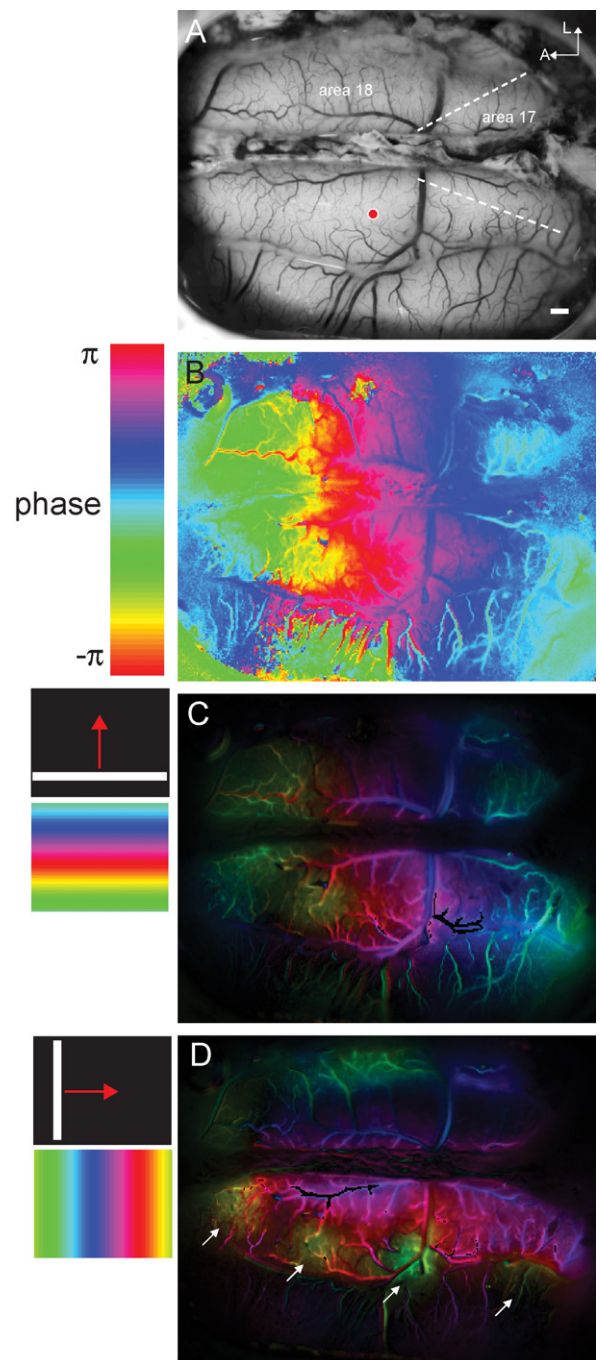


**Fig. 3.** (A) Vasculature pattern in the ROI of the visual cortex in case 1. Borders between areas 17 and 18, based on spatial frequency maps, are indicated by dotted lines. (B) Phase map at the frequency of stimulation for a horizontal bar. (C, D) Map of the phase normalized by the magnitude for horizontal and vertical moving bars. White arrows indicate convergence to the extreme lateral parts of the visual field. Scale bar = 1 mm.

displays the spectral responses to four horizontal bars moved in the same direction at different stimulus frequencies (arrows), for five distinct recording sessions (boxes 1–5). The stimulus can be appreciated in [supplementary video 6](#). The five experiments were combined to provide 19 measures of the HRF at frequencies varying between 0.03 and 0.5 Hz (Fig. 6, panel A). The HRF was estimated in the frequency domain, the maximum spectral response was measured between 0.1 and 0.15 Hz and no response was observed past 0.5 Hz as previously assumed. This amplitude profile was fitted with the frequency profile of multi-Gaussian-components HRF with the

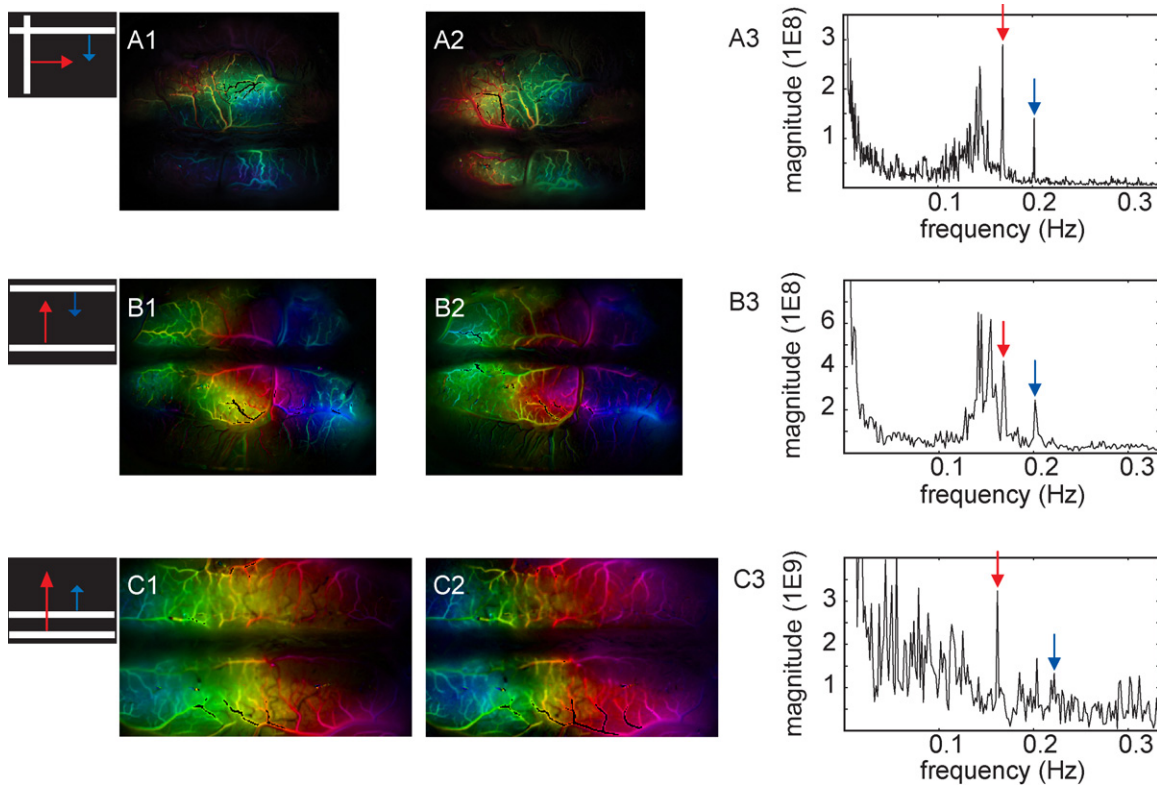


**Fig. 4.** Relative maps along (A1) the azimuth and (A2) elevation obtained in the same recording session from case 2. The stimulus consisted of two perpendicular bars moving at two frequencies (0.167 and 0.2 Hz). (A3) Magnitude spectrum with responses identified by arrows. (B) Relative maps along elevation obtained in the same recording session from case 1 with two parallel bars moving up- and downward at two frequencies (0.167 and 0.2 Hz). (C) Relative maps along elevation obtained by 2 bars moving upward at two frequencies in the same recording session (0.16 and 0.22 Hz, case 3). Note that the phases were aligned in panels B and C for clarity. Scale bar = 1 mm.

method described in equation (B.2) of Appendix B (panel B). Three parameters are fit for each Gaussian component in addition of a single overall offset. The best fit was obtained with a 4-Gaussian model when compared to 2- or 3-Gaussians models. As discussed in the appendix, the fit to a parameterized model is necessary since only amplitude data is used. It should be noted that with this method, the fits are valid up to a phase (temporal shift in the HRF), only the shape of the response can be fit as discussed in Appendix B. An episodic protocol of HRF was measured independently to validate this periodic-based HRF estimation (panel B). A close match was observed between episodic and periodic HRF in the spectral domain.

The spectral shape of the HRF in each pixel was correlated to the global estimate (i.e., HRF from all pixels) to provide a correlation index evaluating the homogeneity of the HRF. Panel C shows the correlation map which illustrates the similarity of the HRF across different regions of the cortex. Under large zone of equivalent illumination (e.g. comparable SNR), the correlation (i.e. homogeneity) were high and constant ( $r > 0.8$ ) and covered the transition zone between areas 17 and 18. A similar homogeneity of the HRF was observed for a second dataset (case 4, not shown). In addition to the correlation, the ratio  $|HRF(\omega_1)|/|HRF(2\omega_1)|$  appearing in (9) was calculated (supplementary Fig. 3). These ratios showed that there was a high degree of homogeneity on a large portion of the cortex in two cases both with periodic (panels A and B) and episodic paradigms (panels C and D). All these results clearly indicate that the HRF is homogeneous in the cat primary visual cortex and that the ratio of the second to the first harmonic can be used to directly evaluate maps of pRF (see (12) in the model). It should be noted that this validation is academic in nature since the amount of time and number of experiments necessary to evaluate the HRF in continuous stimulation is much larger than with episodic paradigms.

However, the good correspondence with the episodic waveform confirms that the episodic HRF can be used to calibrate continuous stimulation measures.

### 3.3. pRF estimation

The main goal of the study was to demonstrate that our proposed model can be used to estimate the receptive field size of the underlying population of neurons. As mentioned above, the simple estimation of the first harmonic does not provide information about the shape of the response. Additional knowledge can be gathered however by using a ratio of the second harmonic relative to the first when the HRF is considered constant throughout the cortex, which was demonstrated above. Panel B in Fig. 7 illustrates the responses at both first and second harmonics to horizontal bars moving at various frequencies (0.05–0.333 Hz) in areas 17 and 18 (panel A). Due to the frequency dependence of the HRF (see above), the magnitude was maximum at 0.111 Hz for the first harmonic and at 0.1 Hz (stimulus frequency = 0.05 Hz) for the second, independently of the cortical location. Panel C shows the ratio of the second harmonic relative to the first, a measure that is inversely related to the pRF (see (9) in the model); for low stimulus frequencies, this ratio was always higher in the posterior part of the cortex (area 17). Fig. 8 illustrates the spectra and magnitude averages in the two regions of interest shown in red and blue boxes in Fig. 7C. The spectrum of the response in areas 17 (panel A) and 18 (panel B) confirmed the previous observation that the second harmonic became smaller when the stimulus frequency increased and that the second to first harmonic ratio was always stronger in area 17 than in area 18. The previous data can also be presented as a function of stimulus frequency. Panel A of Fig. 9 clearly shows that the ratio was all the time higher in area 17 and was always greater for low stimulus frequen-

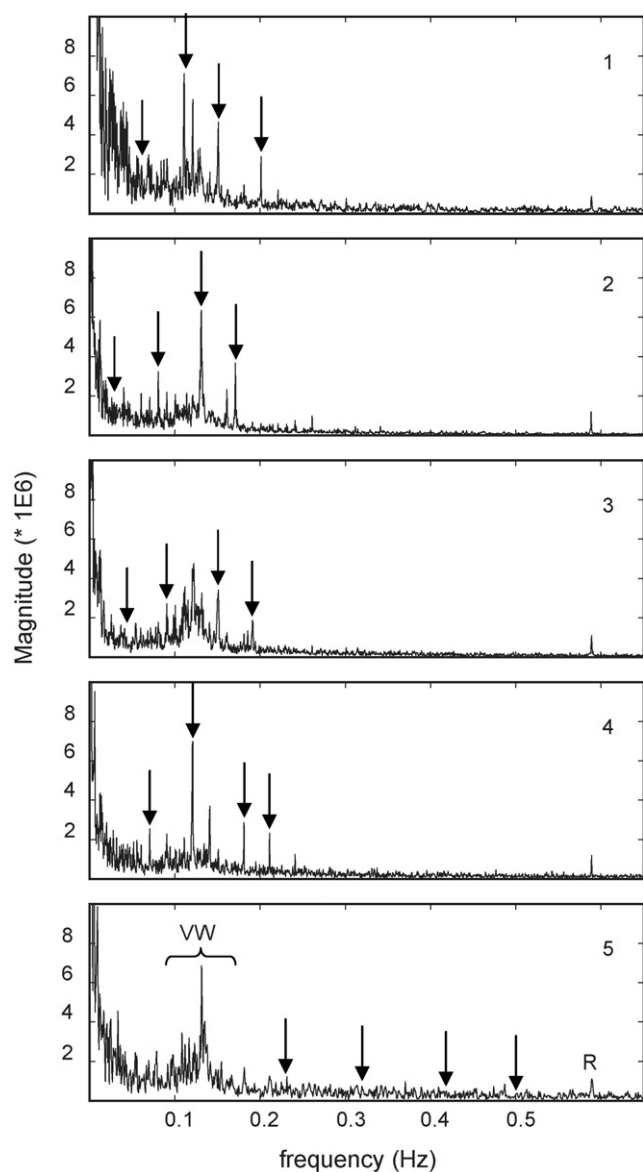


**Fig. 5.** Magnitude spectrum in five recordings from case 3 following stimulation with a set of 4 bars moving at four different frequencies indicated by the black arrows: recording 1 (0.06, 0.11, 0.15 and 0.2 Hz), recording 2 (0.03, 0.08, 0.13 and 0.17 Hz), recording 3 (0.04, 0.09, 0.15 and 0.19 Hz), recording 4 (0.07, 0.12, 0.18 and 0.21 Hz) and recording 5 (0.23, 0.32, 0.42 and 0.50 Hz). Recording time was 30 min in 1–4 and 18 min in 5. These data correspond to the average signal magnitude of all pixels on the cortical region presented in Fig. 6C.

cies, irrespective of the area considered. All these results could be reproduced over time (compared values in panels A and B obtained one day apart in the same cat) and across animals (panel C).

To validate the relation between the second to first harmonic ratio and the pRF, the former was compared with the spatial frequency selectivity map. The underlying assumption was that spatial frequency is related to the pRF size. To obtain spatial frequency selectivity maps, orientation maps corresponding to the difference of activation between vertical and horizontal gratings were acquired at eight spatial frequencies (supplementary Fig. 4, panel A). Activations were maximal at 0.35 and 0.15 c/deg in areas 17 and 18, respectively. The absolute values displayed at the pixel level in each area show that a high degree of spatial frequency selectivity can be measured by optical imaging (supplementary Fig. 4, panel B). Panel A4 of Fig. 10 shows the resulting map in which the spatial frequency which evoked the strongest response (i.e., optimal

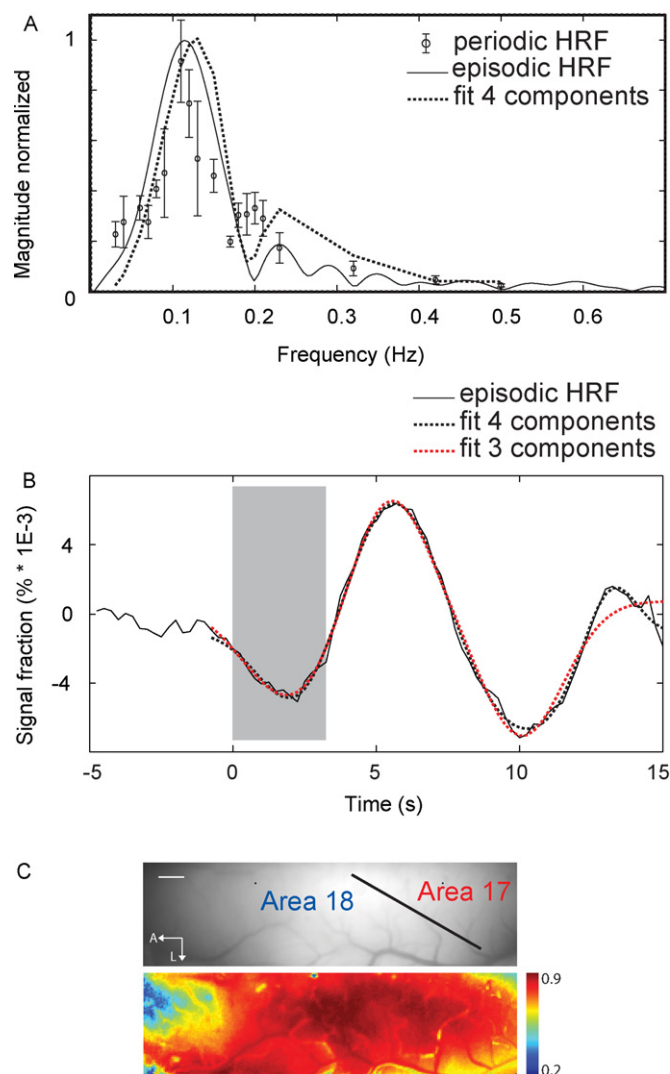


**Fig. 6.** (A) Mean and standard deviation of the normalized response (circles, obtained from Fig. 5), fitted by four Gaussian canonical HRF models (dashed line), and compared with the Fourier transform of an episodic HRF (continuous line). (B) Episodic HRF (black line) and canonical HRF model constituted by 3 Gaussians (red dashed line) and 4 Gaussians (black dashed line). (C) HRF correlation across the imaged cortex. (For interpretation of the references to color in this figure legend, the reader is referred to the web version of the article.)

spatial frequency) was measured for each pixel. Mapping spatial frequency from two differential orientation maps will necessarily lead to incomplete spatial frequency maps. Since oblique orientation domains were not activated, a number of pixels did not display a spatial frequency tuning, increasing noise level in the spatial frequency map. Panel A2 displays the spatial frequency normalized by the amplitude, which allows accurate spatial frequency measurements in activated orientation domains (e.g. cardinal orientations). Note however that this partial spatial frequency coverage does not allow corroborating (or not) the presence of spatial frequency maps as those shown by Issa et al. (2000). Optimal spatial frequency was 0.3–0.5 c/deg in area 17 and 0.1–0.2 c/deg in area 18. These values are comparable to those previously obtained by electrophysiological (Movshon et al., 1978: A17 (median)=0.7, A18=0.18), and optical imaging means (Issa et al., 2000: A17 (median)=0.53, A18=0.18). The differences between area 17 values are likely to come from pixels located in the Transition Zone between areas 17 and 18, which can exhibit “mixed” properties of both areas.

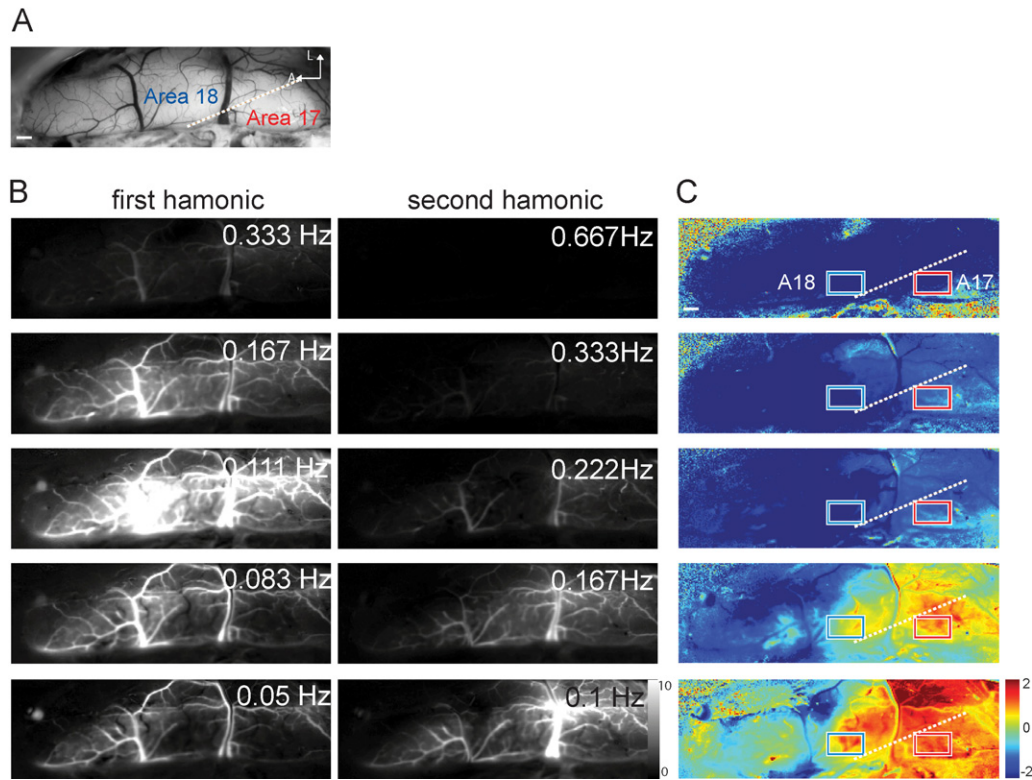


**Fig. 7.** (A) Vasculature pattern in the ROI of case 4. (B) Magnitude maps of the response for an upward bar at the first and second harmonics for five stimulus frequencies: 0.333, 0.2, 0.167, 0.083 and 0.05 Hz (i.e. 1/3 s, 1/6 s, 1/9 s, 1/12 s and 1/20 s). (C) Maps of the second to the first harmonic ratio for the five frequencies used in B. Dotted lines indicate the approximate delimitation between areas 17 and 18. Scale bar = 1 mm.

The relation between optimal spatial frequencies (map in panel A) and the ratio of the second harmonic to the first (map at 0.167 Hz in panel C of Fig. 7) is shown for each pixel in panel B. A positive relation between spatial frequency and harmonic ratio could be observed: high optimal spatial frequency in area 17 was associated with high ratio, meaning small pRF in our model. In contrast, in area 18, low optimal frequencies were associated with low ratios, meaning large pRFs. This positive correlation was also observed with ratio associated to other stimulus frequencies (0.05–0.167 Hz, supplementary Fig. 5).

Given that the HRF is equally distributed throughout the cortex, the quantification of ratio of second/first harmonic allowed to successfully compare the pRF size between two area by using (12). This new measure can yield significant benefits in visual pathology situations as it can be used to quantify the effect of experimental manipulations on the pRF size. Although this relative quantification was robust, the quantification of individual values of pRF in one area through (9) was more challenging (data not shown) mainly due to baseline noise. Further work is being done to address those difficulties.

#### 4. Discussion

This study showed that the “continuous stimulation paradigm” developed by Kalatsky and Stryker (2003), can be successfully used to acquire visuotopic maps along the azimuth and elevation using vertical and horizontal bright bars in the cat primary visual cortex, with reduced acquisition time. More important perhaps is the evidence that, in the same recording session, up to four stimuli presented at different frequencies can be combined to evaluate the profile of the HRF. The latter was homogeneous throughout the cortex allowing the relative estimation of the pRF size between two areas by simply computing the ratio of the second to the first har-

monic. Our model shown that this ratio was inversely proportional to the pRF size and was found to be stronger in area 17 than 18. Spatial frequency was used to validate this measure and confirmed that high ratio pixels are associated with high spatial frequencies.

##### 4.1. Visuotopic mapping by single harmonic analysis

While the episodic method has been successfully used to acquire visuotopic maps in rodents and tree shrews (Bosking et al., 2002, 2000; Gias et al., 2005; Schuett et al., 2002; Van Hooser et al., 2005), limitations of this paradigm include coarse definition of the maps and long recording sessions. The recently developed continuous stimulation paradigm was, until now, essentially applied to rodent models (Cang et al., 2005a,b; Kalatsky and Stryker, 2003). In the present study, we demonstrated that this method is suitable for high-resolution visuotopic mapping of the cat cortex. The rationale behind the present work was the observation that, while continuous visuotopic signals can be obtained rapidly, these signals provide rather limited information. Here, higher harmonics were used for the first time to evaluate the HRF and the pRF size. This yielded the acquisition of maps with a resolution at the sub-millimeter scale. The general organization of the visuotopic maps obtained in this study was comparable to those previously reported using other approaches such as electrophysiological mapping (Albus and Beckmann, 1980; Olman et al., 2003; Tusa et al., 1978; Tusa et al., 1979). A clear continuous organization of elevation was systematically observed on the primary visual cortex, mainly comprising the lower visual field representation in area 18. A continuous organization of the azimuth was also observed.

The use of horizontal or vertical oriented moving bars in animals with a cortical columnar organization for orientation raises the question of the homogeneity of activation. One could have expected to observe patches of activities within the visuotopic maps. This

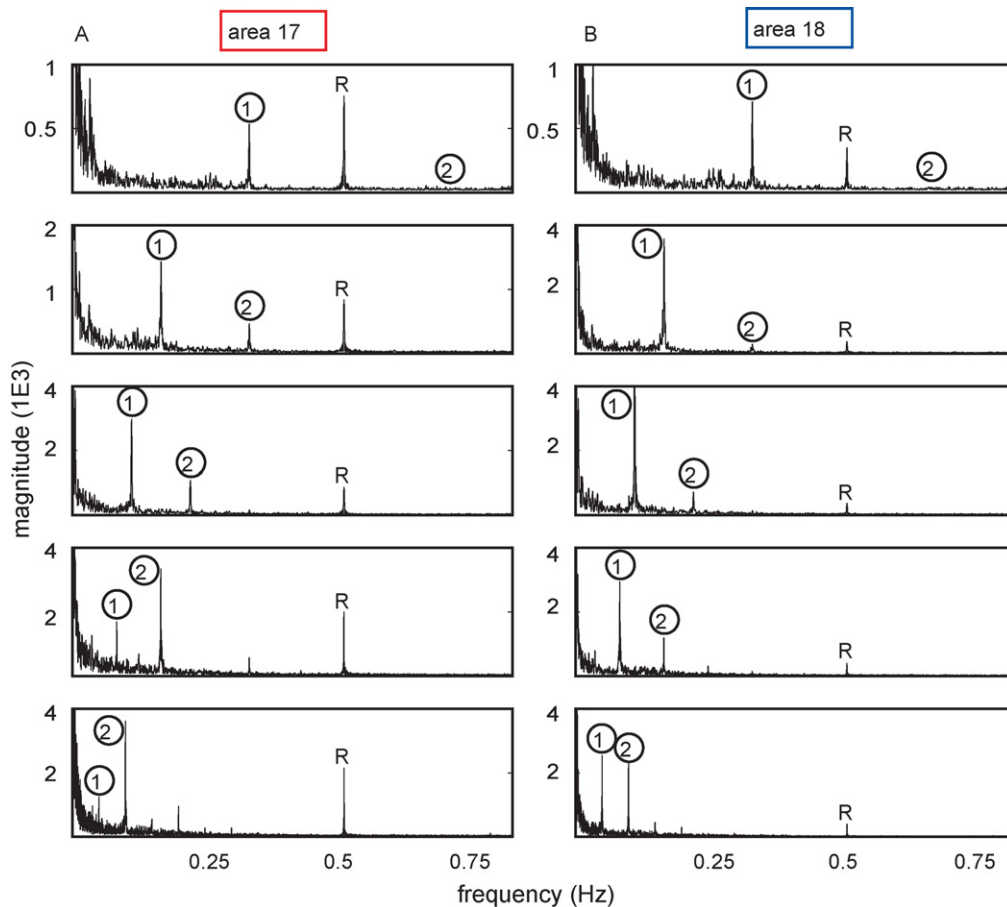


**Fig. 8.** Magnitude spectrum in the two ROIs indicated in Fig. 7C (red and blue squares for areas 17 and 18). (For interpretation of the references to color in this figure legend, the reader is referred to the web version of the article.)

was not the case, suggesting that optical imaging responses to bars were dominated by non oriented signals. Similarly, no evidence of modular organization for ocular dominance was seen in area 17 despite the fact that the stimuli were presented monocularly.

#### 4.2. Hemodynamic response and noise

Combining continuous recording with spectral decomposition represents a powerful method since noise can be easily discriminated from the raw signal because of its periodicity, e.g. around 3 Hz for heartbeat (generally filtered), 0.5 Hz for respiration and 0.1 Hz for vasomotion. In our experiments, a major noise contribution originated from vasomotion which correspond to slow pulsations of oxygenated blood in the capillaries of anesthetized and awake animals. These waves emerged from various loci in the cortex and had a frequency slightly greater than those reported in previous studies in the same species (0.12–0.14 Hz against 0.1 Hz or less in (Kalatsky and Stryker, 2003; Mayhew et al., 1996)). The contribution of vasomotion noise was reduced by adjusting the stimulus frequencies to values away from the noise frequencies.

By choosing different stimulus frequencies, we assumed that the optical response is additive for independent stimuli and therefore extracted the distinct responses in the same recording session (Kalatsky et al., 2006). With this assumption, multiple visuotopic maps were acquired simultaneously in a single recording session. This paradigm was exploited to measure the HRF frequency response by blending different frequencies in a session. A close relationship was observed between the HRF derived from continuous and episodic protocols in both time and frequency domains despite the fact that the stimuli were different (bars and sine wave

gratings). The HRF had its maximum value around the same frequency as vasomotion and was homogeneous in a large portion of the cortex, independently of the visual area considered or the density of the vasculature (but see (Harrison et al., 2002)). The few non-homogeneities observed could be attributed to a non-uniform illumination level yielding then different SNRs.

The HRF evaluation was based on a number of assumptions. Several factors could have yielded a misevaluation of this measure: the number of bars, their speed and frequency. In our approach, we assumed that the velocities used (0.03–0.5 Hz corresponding to 2.7–45 deg/s) did not influenced the neuronal responses, which is an incorrect statement if one considers the bulk of electrophysiological data on this matter. In particular, when several bars were presented, the neuronal response to the highest frequencies (0.2–0.5 Hz) can be reduced, displacing the HRF estimate to lower frequency. This last observation may explain, in part, that the quantification of individual values of pRF was not achieved from (9). However, the normalization with common frequencies chosen between pairs of experiments performed in our five sets of multiple stimulations reduced the impact of the detrimental effects observed at high frequency stimulations. Thus, in our paradigms, velocity and frequency appear not to be critical. The maximum value of the HRF was around 0.1 Hz (10 deg/s), in agreement with episodic measures, and no differences in the HRF profile were observed along the transition from area 18 to 17, where neurons are tuned to slower velocities. It is also noticeable that the ratio  $|HRF(\omega_1)|/|HRF(2\omega_1)|$  was always homogeneous throughout the cortex in a large range of frequencies (0.05–0.33 Hz). It thus can be concluded that speed selectivity played a minor role in HRF profiles.

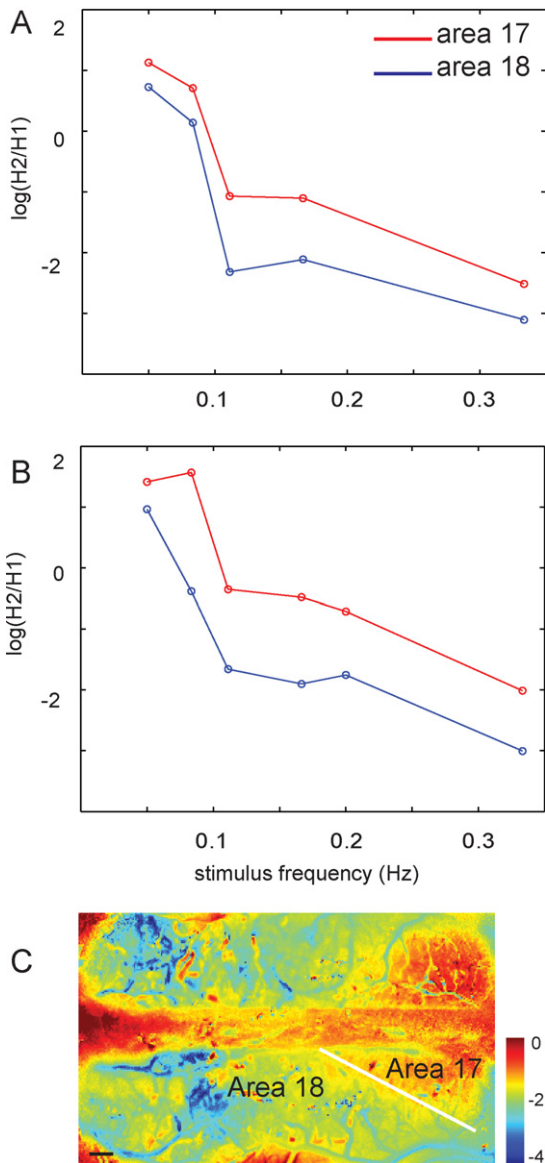


**Fig. 9.** (A) Ratio of the second to the first harmonic in the two ROIs indicated in Fig. 7C as a function of the five stimulus frequencies. (B) Data from another experiment carried out one day later in the same animal (case 4) shows the stability of the measures. (C) Maps of the second to first harmonic ratios at 0.167 Hz obtained in another animal (case 3). Scale bar = 1 mm.

Finally, as expected, the HRF did not carry neuronal information beyond 0.5 Hz; thus continuous stimulation applied to intrinsic signals cannot be used for stimulation periods shorter than 2 s.

#### 4.3. Response bandwidth by multiple harmonics analysis

According to the model, the ratio of the second to the first harmonic carries information about the profile of the neuronal response. The multiple harmonics analysis was used to evaluate the relative size of the pRF. For each stimulus frequency tested, the ratio was always larger in area 17 than in 18. Further, this ratio was greater in parts of area 18 representing the peripheral visual field where receptive fields are known to be larger in size. Similar observations were reported in human fMRI studies, with the comparable periodic paradigm (Engel et al., 1994; Tootell et al., 1997). These authors did not spectrally decompose the signal the same way as we did. Nevertheless, they noted a different time course between areas V1 and V3, supporting the presence of different receptive field

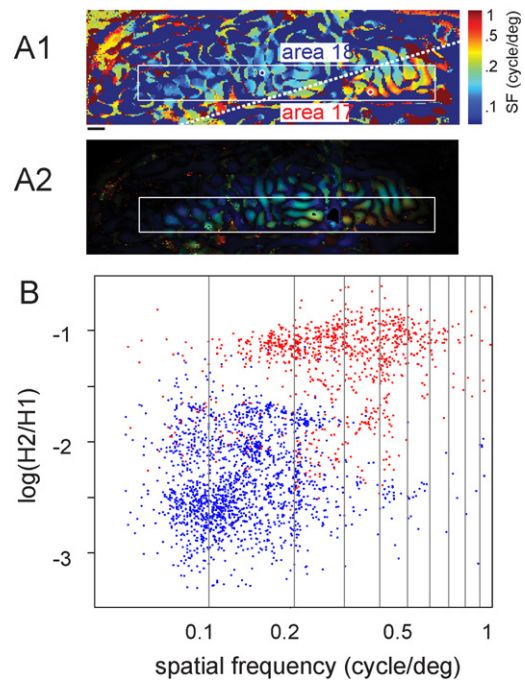


**Fig. 10.** (A) Optimal spatial frequency map from case 4 (panel 1: spatial frequency alone; panel 2: normalized by amplitude). The white rectangle indicates the ROI of the scatter plot made in (B). The dotted line indicates the border between areas 17 and 18 based on the transition of optimal spatial frequency. (B) Correlation between the spatial frequency and the ratio shown in Fig. 7C (0.167 Hz). Red and blue dots indicate band-pass pixels from areas 17 and 18, respectively (as delimited in panel A). Scale bar = 1 mm. (For interpretation of the references to color in this figure legend, the reader is referred to the web version of the article.)

sizes in those areas. Based on this observation, a recent approach was proposed by (Dumoulin and Wandell, 2008) who estimated the pRF size in each voxel by a linear spatio-temporal model of the fMRI response. As in the present study, the pRF was modeled by a Gaussian function and the neuronal response was convolved by the HRF. This method gives an absolute estimation of the pRF but assumes that the contribution of physiological noise must be minimal in order to fit the data with the model. This is not the case in optical imaging (see the dominant contribution of noise in Fig. 2). The method proposed in this work has the advantage of being independent of the noise model chosen and straightforward in its application.

The quantification of the ratio *per se* did not allow a direct quantification of the pRF size. Indeed, if one considers only a Gaussian neuronal response without any HRF, the ratio should be constant for any frequency of stimulation. But, as shown in the model, the multiplication of the HRF in the frequency space (i.e., temporal convolution of the signal by the HRF) modified the ratio as a function of the stimulus frequency. The HRF profile is such that the second harmonic contribution is inversely proportional to the stimulus frequency. Thus, to estimate the ratio, the frequency of stimulation should be reduced while the number of repetitions should be maximized, avoiding the physiological sources of noise. At low stimulus frequency (0.05 Hz), third and fourth harmonics were also observed and one could envision using these additional components for quantifying neuronal response profiles. Finally, one should keep in mind that, as described in the model, relative or absolute estimation of pRF is not equivalent to a direct quantification of individual receptive field size. Thus, the pRF variation can be due, in part, to a difference in position variance of receptive fields between areas (Dumoulin and Wandell, 2008).

The relevance of the ratio as an indirect measure of the pRF size has been validated by measuring spatial frequency tuning for each

pixel. As such, a positive correlation between the ratio and the spatial frequency was found in the primary visual cortex (in both areas 17 and 18). It should be kept in mind that when using a flat screen, a bar presented in the periphery of the visual field appears to move slower, yielding an overestimation of the pRF. This effect can be particularly significant for eccentricities greater than 30°, but would be less pronounced in cats than rodents which have a larger monocular field of view. Another source of uncertainty could come from the fact that neurons with similar optimal spatial frequencies may have different receptive field sizes, reducing then the correlation between optimal spatial frequency and pRF estimate.

A 5° width bar was used to successfully image and evaluate the pRF size in areas 17 and 18. This width value closely matches receptive field size in area 18 but is greater than that reported in area 17 (Albus and Beckmann, 1980; Olman et al., 2003; Tusa et al., 1978, 1979). However, as previously described, due to the “point spread” response in optical imaging, the response at each pixel is more associated to the pRF, which covers a larger spatial area than an individual receptive field. We then assumed that the width of the bars was always smaller than the pRF and consequently that it did not notably interfere with the evaluation of the latter.

## 5. Conclusion and future directions

Using continuous stimulation, clear visuotopic maps of the cat primary visual cortex were acquired in a short recording period and responses to mixed stimuli were simultaneously recorded in a given test. More important perhaps, the analysis of higher harmonics was exploited to estimate the receptive fields' size of the underlying neurons. This measurement represents a new tool that will likely be valuable in projects requiring a thorough quantification of cortical organization (e.g. developmental studies, impact of experimental manipulations on functional maps).

The study presents a new approach to measure the shape of a response (i.e. the bandwidth of the Gaussian model of the receptive field). This approach can be easily exported to parameters other than receptive field size, and that, for any moving stimulus (e.g., wedge or ring as those used in fMRI). A particular example would be the evaluation of orientation tuning bandwidth in response to rotating grating (as used in (Kalatsky and Stryker, 2003), see Figs. 2G–H and 8, (Vanni et al., 2009)). It will also be very useful in other optical imaging approaches such as those based on flavo-protein autofluorescence and voltage sensitive dyes (Husson et al., 2007). It would as well be beneficial in studies investigating other sensory systems (e.g., tonotopic bandwidth in the auditory cortex, Kalatsky et al., 2005). Finally, the bandwidth estimation could also be exploited in human imaging modalities such as fMRI or diffuse optical imaging given the similar nature of the signals recorded.

## Acknowledgments

This work was supported by NSERC and CIHR grants to C.C. and a NSERC grant to F.L. FRSQ provided part of C.C.'s salary (Chercheur National program). MV was supported in part by “Foreign Affairs and International Trade” and “Faculté des études supérieures” fellowships. JP was supported by a NSERC scholarship. We are grateful to J. Ribot for his comments on the manuscript.

## Appendix A.

In this appendix, details are provided on the academic model of perfectly specific neurons. Consider a group of neurons that reacts only when a horizontal bar is located at a very precise position on a screen, i.e. having a very small receptive field. In this case,  $R\{s(t)\}$  can be modeled as a Dirac distribution located on that position.

The bar will pass through that point  $N$  time,  $N$  being the number of periods of the stimulation. Each of these occurrences can be related to a particular time  $\tau_{ij} + nT$  in the experiment, where  $\tau_{ij}$  is the first time when the response occurs within the period and  $nT$  is the  $n$ th period of the stimulus. The index  $\{ij\}$  indicates quantities that are specific to a pixel (therefore to a group of neurons). The idealistic period-normalized neural response to a preferred stimulus can be modeled by

$$R_{ij} \left\{ s(t; \omega_1) \right\} (t) = \sum_{n=0}^N \delta(t - nT - \tau_{ij}) = \sum_{n=0}^N \delta\left(t - \frac{2\pi}{\omega_1} n - \tau_{ij}\right) \quad (\text{A.1})$$

where  $\omega_1 = 2\pi/T$  is the angular frequency (rad/s) of the stimulus. By taking the Fourier transform:

$$\begin{aligned} \hat{R}_{ij} \left\{ s(t; \omega_1) \right\} (\omega) &= \int_{-\infty}^{\infty} e^{i\omega t} \sum_{n=0}^N \delta\left(t - \frac{2\pi}{\omega_1} n - \tau_{ij}\right) dt = \sum_{n=0}^N e^{-i\omega\left(\frac{2\pi}{\omega_1} n + \tau_{ij}\right)} \\ &= -e^{-i\omega\tau_{ij}} \frac{(1 - e^{-i\omega\left(\frac{2\pi}{\omega_1}(N+1)\right)})}{(1 - e^{-i\omega\left(\frac{2\pi}{\omega_1}\right)})} \\ &= e^{-i\omega\tau_{ij}} e^{-i\pi\frac{\omega}{\omega_1} N} \frac{\sin\left[\frac{\omega}{\omega_1}\pi(N+1)\right]}{\sin\left[\frac{\omega}{\omega_1}\pi\right]} \end{aligned} \quad (\text{A.2})$$

Where the geometric progression was used to get the last line. In continuous stimulation, the frequency of interest is  $\omega = \omega_1$  and, neglecting the noises in (1) assuming a small spectral width, the measured response can be identified in the Fourier domain by a simple product of the HRF and the response  $R_{ij}$  at the frequency of stimulation. By using l'Hôpital's rule on (A.2), the strength of the harmonic located at  $\omega_1$ , the stimulation frequency, is seen to be linearly dependant on  $N$ :

$$\hat{R}_{ij} \left\{ s(t; \omega_1) \right\} (\omega_1) = (-1)^N e^{-i\omega_1\tau_{ij}} (N+1) \quad (\text{A.3})$$

This can be extended to the case of more than one (two in this example) periodic stimulus of angular frequencies  $\omega_1$  and  $\omega_2$  respectively, by assuming linearity, we have for experiment time  $2\pi N/\omega_1$ :

$$\begin{aligned} R_{ij} \left\{ \sum_{k=1}^{nstim} s_k(t; \omega_k) \right\} (t) &= A \sum_{n=0}^N \delta(t - t_n - \tau^{(1)}) \\ &+ B \sum_{k=0}^M \delta(t - t_k - \tau^{(2)}) + \dots \end{aligned} \quad (\text{A.4})$$

Where  $(2\pi M/\omega_2) < (2\pi N/\omega_1)$ , since the stimuli are considered to not be multiples of each other, the remainder containing the response for the partial presentation of stimulus with amplitude  $B$ . In the following this is described by an  $O(1)$  term (compared to  $O(N)$  and  $O(M)$  terms). The Fourier transform for fixed experiment time yields:

$$\begin{aligned} \hat{R}_{ij} \left\{ \sum_{k=1}^{nstim} s_k(t; \omega_k) \right\} (\omega) &= A e^{-i\omega\tau_{ij}^{(1)}} e^{-i\pi\frac{\omega}{\omega_1} N} \frac{\sin\left[\frac{\omega}{\omega_1}\pi(N+1)\right]}{\sin\left[\frac{\omega}{\omega_1}\pi\right]} + \\ &A e^{-i\omega\tau_{ij}^{(2)}} e^{-i\pi\frac{\omega}{\omega_2} N} \frac{\sin\left[\frac{\omega}{\omega_2}\pi(M+1)\right]}{\sin\left[\frac{\omega}{\omega_2}\pi\right]} + O(1) + \dots \end{aligned} \quad (\text{A.5})$$

Applying l'Hôpital's rule at either  $\omega = \omega_1$  or  $\omega = \omega_2$  (or any  $n$ ) will yield equations (13).

## Appendix B.

Since only amplitude data is used for the recovery of the HRF, a parametrized model of the HRF is built by introducing  $N$  Gaussian components:

$$h(\alpha, a_i, b_i, c_i; t) = \alpha + \sum_{k=1}^N a_i \exp\left(-\frac{(t - b_k)^2}{2c_k^2}\right) \quad (\text{B.1})$$

To describe each component, three parameters are needed in addition to an overall parameter,  $\alpha$ , describing a data offset. By Fourier transforming this functional form and evaluating the modulus of the Fourier transform at experimental frequencies,  $\omega_k$ , it is possible to minimize the least square distance between the parametrized form and the experimental data:

$$\Omega = \sum_k \left( \left| \widehat{HRF}(\omega_k) \right| - \left| h(\alpha, a_i, b_i, c_i; \omega_k) \right| \right)^2 \quad (\text{B.2})$$

Since absolute values are used, this minimization does not completely determine the model. If all  $b_k$  are shifted by a constant,  $\delta$ , then the Fourier transform of the sum (B.1) will be modified by a pure phase at each frequency and this change will be invisible in the minimization problem (B.2). This shift amounts to an overall translation in time thus the estimation presented in the results cannot recover this overall shift. However if a single Gaussian function in the sum (B.1) is temporally shifted, the modulus at the experimental frequencies will be modified since the absolute value of the sum is used in the Fourier domain (and not the sum of the absolute values). Thus the relation between the different terms, or the shape of the HRF, can be recovered by using three or four Gaussian components as shown in the results.

## Appendix C. Supplementary data

Supplementary data associated with this article can be found, in the online version, at doi:10.1016/j.jneumeth.2010.03.013.

## References

- Albus K. A quantitative study of the projection area of the central and the paracentral visual field in area 17 of the cat. I. The precision of the topography. *Exp Brain Res* 1975;24:159–79.
- Albus K, Beckmann R. Second and third visual areas of the cat: interindividual variability in retinotopic arrangement and cortical location. *J Physiol* 1980;299:247–76.
- Bishop PO, Kozak W, Vakkur GJ. Some quantitative aspects of the cat's eye: axis and plane of reference, visual field co-ordinates and optics. *J Physiol* 1962;163:466–502.
- Blasdel GG. Differential imaging of ocular dominance and orientation selectivity in monkey striate cortex. *J Neurosci* 1992;12:3115–38.
- Bonhoeffer T, Grinvald A. Optical imaging based on intrinsic signal – the methodology. In: Toga AW, Mazziotta JC, editors. *Brain mapping: the methods*; 1996.
- Bosking WH, Crowley JC, Fitzpatrick D. Spatial coding of position and orientation in primary visual cortex. *Nat Neurosci* 2002;5:874–82.
- Bosking WH, Kretz R, Pucak ML, Fitzpatrick D. Functional specificity of callosal connections in tree shrew striate cortex. *J Neurosci* 2000;20:2346–59.
- Buzas P, Volgushev M, Eysel UT, Kisvarday ZF. Independence of visuotopic representation and orientation map in the visual cortex of the cat. *Eur J Neurosci* 2003;18:957–68.
- Cang J, Kaneko M, Yamada J, Woods G, Stryker MP, Feldheim DA. Ephrin-as guide the formation of functional maps in the visual cortex. *Neuron* 2005a;48:577–89.
- Cang J, Renteria RC, Kaneko M, Liu X, Copenhagen DR, Stryker MP. Development of precise maps in visual cortex requires patterned spontaneous activity in the retina. *Neuron* 2005b;48:797–809.
- Chen-Bee CH, Agoncillo T, Xiong Y, Frostig RD. The triphasic intrinsic signal: implications for functional imaging. *J Neurosci* 2007;27:4572–86.
- Ciuciu P, Poline JB, Marrelec G, Idier J, Pallier C, Benali H. Unsupervised robust nonparametric estimation of the hemodynamic response function for any fMRI experiment. *IEEE Trans Med Imaging* 2003;22:1235–51.
- Cohen-Adad J, Chapuisat S, Doyon J, Rossignol S, Lina JM, Benali H, et al. Activation detection in diffuse optical imaging by means of the general linear model. *Med Image Anal* 2007;11:616–29.
- Cynader MS, Swindale NV, Matsubara JA. Functional topography in cat area 18. *J Neurosci* 1987;7:1401–13.

- Das A, Gilbert CD. Distortions of visuotopic map match orientation singularities in primary visual cortex. *Nature* 1997;387:594–8.
- Das A, Gilbert CD. Long-range horizontal connections and their role in cortical reorganization revealed by optical recording of cat primary visual cortex. *Nature* 1995;375:780–4.
- Dumoulin SO, Wandell BA. Population receptive field estimates in human visual cortex. *NeuroImage* 2008;39:647–60.
- Dunn AK, Devor A, Dale AM, Boas DA. Spatial extent of oxygen metabolism and hemodynamic changes during functional activation of the rat somatosensory cortex. *NeuroImage* 2005;27:279–90.
- Engel SA, Rumelhart DE, Wandell BA, Lee AT, Glover GH, Chichilnisky EJ, et al. fMRI of human visual cortex. *Nature* 1994;369:525.
- Everson R, Knight BW, Sirovich L. Separating spatially distributed response to stimulation from background. I. Optical imaging. *Biol Cybern* 1997;77:407–17.
- Gabbay M, Brennan C, Kaplan E, Sirovich L. A principal components-based method for the detection of neuronal activity maps: application to optical imaging. *NeuroImage* 2000;11:313–25.
- Gias C, Hewson-Stoate N, Jones M, Johnston D, Mayhew JE, Coffey PJ. Retinotopy within rat primary visual cortex using optical imaging. *NeuroImage* 2005;24:200–6.
- Handwerker DA, Ollinger JM, D'Esposito M. Variation of BOLD hemodynamic responses across subjects and brain regions and their effects on statistical analyses. *NeuroImage* 2004;21:1639–51.
- Harrison RV, Harel N, Panesar J, Mount RJ. Blood capillary distribution correlates with hemodynamic-based functional imaging in cerebral cortex. *Cereb Cortex* 2002;12:225–33.
- Hubel DH, Wiesel TN. Receptive fields, binocular interaction and functional architecture in the cat's visual cortex. *J Physiol* 1962;160:106–54.
- Husson TR, Mallik AK, Zhang JX, Issa NP. Functional imaging of primary visual cortex using flavoprotein autofluorescence. *J Neurosci* 2007;27:8665–75.
- Issa NP, Trepel C, Stryker MP. Spatial frequency maps in cat visual cortex. *J Neurosci* 2000;20:8504–14.
- Kalatsky VA, O'Connor EM, Tcheslavski GV, Kalatsky V. Concurrent multidimensional imaging of visual space representations in mouse visual cortex by Fourier optical imaging of intrinsic signals. *SfN Abstract* 2006; prog. 503.9.
- Kalatsky VA, Polley DB, Merzenich MM, Schreiner CE, Stryker MP. Fine functional organization of auditory cortex revealed by Fourier optical imaging. *Proc Natl Acad Sci USA* 2005;102:13325–30.
- Kalatsky VA, Stryker MP. New paradigm for optical imaging: temporally encoded maps of intrinsic signal. *Neuron* 2003;38:529–45.
- Marrelec G, Benali H, Ciuciu P, Pelegrini-Issac M, Poline JB. Robust Bayesian estimation of the hemodynamic response function in event-related BOLD fMRI using basic physiological information. *Hum Brain Mapp* 2003;19:1–17.
- Mayhew JE, Askew S, Zheng Y, Porrill J, Westby GW, Redgrave P, et al. Cerebral vasomotion: a 0.1-Hz oscillation in reflected light imaging of neural activity. *NeuroImage* 1996;4:183–93.
- Movshon JA, Thompson ID, Tolhurst DJ. Spatial and temporal contrast sensitivity of neurones in areas 17 and 18 of the cat's visual cortex. *J Physiol* 1978;283:101–20.
- Olman C, Ronen I, Ugurbil K, Kim DS. Retinotopic mapping in cat visual cortex using high-field functional magnetic resonance imaging. *J Neurosci Methods* 2003;131:161–70.
- Polimeni JR, Granquist-Fraser D, Wood RJ, Schwartz EL. Physical limits to spatial resolution of optical recording: clarifying the spatial structure of cortical hypercolumns. *Proc Natl Acad Sci USA* 2005;102:4158–63.
- Schuetz S, Bonhoeffer T, Hubener M. Mapping retinotopic structure in mouse visual cortex with optical imaging. *J Neurosci* 2002;22:6549–59.
- Sornborger A, Sailstad C, Kaplan E, Sirovich L. Spatiotemporal analysis of optical imaging data. *NeuroImage* 2003;18:610–21.
- Sornborger A, Yokoo T, Delorme A, Sailstad C, Sirovich L. Extraction of the average and differential dynamical response in stimulus-locked experimental data. *J Neurosci Methods* 2005;141:223–9.
- Tootell RB, Mendola JD, Hadjikhani NK, Ledden PJ, Liu AK, Reppas JB, et al. Functional analysis of V3A and related areas in human visual cortex. *J Neurosci* 1997;17:7060–78.
- Tusa RJ, Palmer LA, Rosenquist AC. The retinotopic organization of area 17 (striate cortex) in the cat. *J Comp Neurol* 1978;177:213–35.
- Tusa RJ, Rosenquist AC, Palmer LA. Retinotopic organization of areas 18 and 19 in the cat. *J Comp Neurol* 1979;185:657–78.
- Van Hooser SD, Heimerl JA, Chung S, Nelson SB, Toth LJ. Orientation selectivity without orientation maps in visual cortex of a highly visual mammal. *J Neurosci* 2005;25:19–28.
- Vanni MP, Provost J, Casanova C, Lesage F. Bimodal modulation and continuous stimulation in optical imaging to map direction selectivity. *NeuroImage* 2010;49:1416–31.
- Vanni MP, Provost J, Casanova C, Lesage F. Bimodal modulation and continuous stimulation in optical imaging to map direction selectivity. *NeuroImage* 2009;49:1416–31.
- Vanni MP, Villeneuve MY, Provost J, Lesage F, Casanova C. Orientation and direction selectivity in the cat visual cortex by spectral decomposition of the optical imaging signals. *SfN abstract* 2007; prog. 920.11.
- Villeneuve MY, Vanni MP, Casanova C. Modular organization in area 21a of the cat revealed by optical imaging: comparison with the primary visual cortex. *Neuroscience* 2009;164:1320–33.
- Zepeda A, Arias C, Sengpiel F. Optical imaging of intrinsic signals: recent developments in the methodology and its applications. *J Neurosci Methods* 2004;136:1–21.